2014

Interaction of Sine-Gordon Kinks and Breathers With a Parity-Time-Symmetric Defect

Danial Saadatmand
Ferdowsi University of Mashhad

Sergey V. Dmitriev
Institute for Metals Superplasticity Problems RAS

Denis I. Borisov
CC USC RAS

Panayotis G. Kevrekidis
University of Massachusetts Amherst, kevrekid@math.umass.edu

Interaction of sine-Gordon kinks and breathers with a parity-time-symmetric defect

Danial Saadatmand,[1,*] Sergey V. Dmitriev,[2,3,†] Denis I. Borisov,[4,5,‡] and Panayotis G. Kevrekidis[6,§]

[1]*Department of Physics, Ferdowsi University of Mashhad, 91775-1436 Mashhad, Iran*

[2]*Institute for Metals Superplasticity Problems RAS, Khalturin 39, 450001 Ufa, Russia*

[3]*Saint Petersburg State Polytechnical University, Politekhnicheskaya 29, 195251 St. Petersburg, Russia*

[4]*Institute of Mathematics CC USC RAS, Chernyshevsky 112, 450008 Ufa, Russia*

[5]*Bashkir State Pedagogical University, October Rev. 3a, 450000 Ufa, Russia*

[6]*Department of Mathematics and Statistics, University of Massachusetts, Amherst, Massachusetts 01003, USA*

(Received 11 August 2014; published 3 November 2014)

The scattering of kinks and low-frequency breathers of the nonlinear sine-Gordon (SG) equation on a spatially localized parity-time-symmetric perturbation (defect) with a balanced gain and loss is investigated numerically. It is demonstrated that if a kink passes the defect, it always restores its initial momentum and energy, and the only effect of the interaction with the defect is a phase shift of the kink. A kink approaching the defect from the gain side always passes, while in the opposite case it must have sufficiently large initial momentum to pass through the defect instead of being trapped in the loss region. The kink phase shift and critical velocity are calculated by means of the collective variable method. Kink-kink (kink-antikink) collisions at the defect are also briefly considered, showing how their pairwise repulsive (respectively, attractive) interaction can modify the collisional outcome of a single kink within the pair with the defect. For the breather, the result of its interaction with the defect depends strongly on the breather parameters (velocity, frequency, and initial phase) and on the defect parameters. The breather can gain some energy from the defect and as a result potentially even split into a kink-antikink pair, or it can lose a part of its energy. Interestingly, the breather translational mode is very weakly affected by the dissipative perturbation, so that a breather penetrates more easily through the defect when it comes from the lossy side, than a kink. In all studied soliton-defect interactions, the energy loss to radiation of small-amplitude extended waves is negligible.

DOI: 10.1103/PhysRevE.90.052902 PACS number(s): 05.45.Yv, 45.50.Tn

I. INTRODUCTION

The past 15 years have seen a significant series of developments in quantum theory, stemming from the realization by Bender and coauthors that a class of non-Hermitian Hamiltonians possess real spectra under the parity-time ($\mathcal{PT}$) symmetry condition, where parity-time means spatial reflection and time reversal, $x \to -x$ and $t \to -t$ [1,2]. This mathematical discovery has initiated numerous studies of open systems with balanced gain and loss even though the generality of this construction is under discussion [3]. Experimental setups have been offered to create $\mathcal{PT}$-symmetric physical systems in optics [4–8], electronic circuits [9–11], as well as in mechanical systems [12].

In a number of theoretical studies, it has been demonstrated that $\mathcal{PT}$-symmetric systems often demonstrate unusual and counterintuitive properties. These include, among others, unconventional beam refraction [13], Bragg scattering [14], symmetry-breaking transitions [4] and associated ghost states [15–18], a loss-induced optical transparency [5], conical diffraction [19], a new type of Fano resonance [20], chaos [21], nonlocal boundary effects [22], optical switches [23] and diodes [24,25], phase sensitivity of light dynamics [26–28], and the possibility of linear and nonlinear wave amplification and filtering [29–31]. Unexpected instabilities were also identified at the level of $\mathcal{PT}$-symmetric lattices, and nonlinear modes were identified in few-site oligomers, as well as in full lattice settings both in one dimension [32–37] and even in two dimensions [38]. Extensions of $\mathcal{PT}$-symmetric considerations in the setting of active media (of unequal gain and loss) have also recently been proposed [39,40].

Motivated by the linear oscillator problems associated with (linear) electrical [9,10] and mechanical [12] $\mathcal{PT}$-symmetric experiments, Klein-Gordon field-theoretic generalizations with a $\mathcal{PT}$-symmetric defect have been proposed, and the collective variable method has been developed to describe kink dynamics in the system [41]; see also [43,44] for a detailed discussion. It was also shown that standing kinks in such models are stable if they are centered at the loss side of the defect [44], and a standing breather may exist only if centered exactly at the interface between gain and loss regions [45]. A natural question arises about what happens with the moving Klein-Gordon solitary waves when they interact with the spatially localized $\mathcal{PT}$-symmetric defect.

Interaction of solitary waves with each other [46–48] and with local inhomogeneities of media has been attracting the attention of researchers for the past two decades. Interaction of a fluxon with a localized inhomogeneity in a long Josephson junction has been investigated in [49,50]. The reflection windows were observed in the kink-impurity interactions by Fei *et al.* in the sine-Gordon (SG) [51] and ϕ^4 [52] models. Scattering of a SG breather by localized defects has been investigated in the conservative case [53]. It has been shown that the breather can split into a kink and antikink pair or can be accelerated by the defect. This is possible in conservative systems because the translational kinetic energy of the breather

*saadatmand.d@gmail.com

†dmitriev.sergey.v@gmail.com

‡borisovdi@yandex.ru

§kevrekid@math.umass.edu

can be partly converted into its internal energy and vice versa. Scattering of linear and nonlinear waves (solitons) on defects in $\mathcal{PT}$-symmetric optical waveguide arrays was analyzed [24,25,29–31]. It was shown that the incident high-amplitude solitons (or even linear wave packets [24,25]) can excite a mode localized on the $\mathcal{PT}$-symmetric defect. By exciting the localized mode of a large amplitude, it is possible to perform phase-sensitive control of soliton scattering and amplification or damping of the localized mode. The gain-loss pattern in conjunction with the nonlinearity lead to asymmetric propagation of the incoming wave packets depending on their direction of incidence.

Kinks in nonintegrable models such as the perturbed SG equation or the ϕ^4 model can support internal vibrational modes [54]. In some cases, impurities can also support localized vibrational modes. Kinks of the integrable SG equation do not bear internal modes [55]. When a kink hits an impurity in a conservative model, a part of its energy is trapped toward the excitation of the impurity mode [51,56] and another fraction leads to the emission of radiation bursts [57].

A merger of a colliding kink and antikink into a breather is possible in a nonintegrable system when energy loss to radiation and/or excitation of the kink's internal modes is sufficiently large [58–61]. The binding of a free kink and antikink into a breather has been addressed in [62] in the presence of spatially periodic perturbation. An external dc driving force in the absence of damping for a sufficiently large magnitude of the force causes the breather to split into a kink-antikink pair, while for a small driving force the breather excitations lead to stationary modes [63]. The breather can dissociate into a kink-antikink pair under an external field [64]. Conversion of an oscillation mode into a kink-antikink pair has been observed via abrupt distortions of the on-site potential in time or in space [65]. The recent work of [45] illustrated that such an evolution is also possible when the breather is subject to gain, e.g., on the gain side of a $\mathcal{PT}$-symmetric medium.

Interaction of moving solitons with $\mathcal{PT}$-symmetric defects in the realm of the Klein-Gordon field, to the best of our knowledge, has not been studied previously, in part, arguably, since $\mathcal{PT}$-symmetric field theories are a very recent theme of research. In this paper, we aim to reveal the principal physical effects observed during the interaction of SG kinks and breathers with a $\mathcal{PT}$-symmetric defect with balanced gain and loss. In particular, a kink approaching the $\mathcal{PT}$-symmetric defect from the gain side is always transmitted, while from the loss side it may be reflected or transmitted depending on its energy. This suggests an asymmetric effective dynamics that is identified by means of an explicitly solvable collective coordinate approach. We also illustrate how this effective collective dynamics can be modified by the presence of the repulsion from another kink or of the attraction by an antikink. On the other hand, for the breather the dynamics is sensitively dependent on both the characteristics of the breather and those of the defect, potentially exhibiting either gain or loss of energy for the coherent structure (the former possibly even featuring the breakup of the breather into a kink and an antikink waveform).

The structure of the paper is as follows. In Sec. II, following Ref. [41], we introduce the perturbed SG equation and the well-known kink and breather solutions to the integrable SG equation. In Sec. III, a collective variable method is applied and analytically solved to reveal some features of the kink dynamics in the considered system. We then report on the numerical results for scattering of kinks in Sec. IV A, pairs of kinks in Sec. IV B, breathers in Sec. IV C, and kink-antikink pairs in Sec. IV D. Our conclusions and some future directions are presented in Sec. V.

II. THE MODEL

We consider the perturbed sine-Gordon equation of the form [41]

$$a\phi_{tt} - b\phi_{xx} + c\sin\phi = d\gamma(x)\phi_t, \tag{1}$$

where $\phi(x,t)$ is the unknown scalar field, lower indices denote partial differentiation, and a, b, c, and d are the coefficients. For instance, in a pendulum setting where ϕ plays the role of an angular variable in the long-wavelength limit (see, e.g., [42]), a may correspond to the moment of inertia, b to the coupling between pendula, c to the torque due to gravity, and d to the dashpot type of gain/loss prefactor. The latter constitutes also the perturbation term on the right-hand side of the equation. In terms of new variables $\phi \to (A^2ac/d^2)\phi$, $t \to (Aa/d)t$, and $x \to (A\sqrt{ab}/d)x$, Eq. (1) assumes the dimensionless form

$$\phi_{tt} - \phi_{xx} + \sin\phi = A\gamma(x)\phi_t. \tag{2}$$

The parameter A controls the perturbation amplitude. To study the effects of a spatially localized $\mathcal{PT}$-symmetric defect on traveling kinks and breathers, for the function $\gamma(x)$ we take

$$\gamma(x) = \{\exp[-\beta(x+\delta)^2] - \exp[-\beta(x-\delta)^2]\}, \tag{3}$$

which has the symmetry $\gamma(-x) = -\gamma(x)$. This ensures that Eq. (3) is $\mathcal{PT}$-symmetric, physically implying that while Eq. (2) describes an open system with gain and loss, the gain balances the loss. The gain-loss spatial profile determined by Eq. (3) represents a superposition of two bell-shaped functions with the separation between them controlled by the parameter δ. The parameter β is related to the hump inverse width. For $A = 0$ and/or $\delta = 0$, one has $\gamma(x) \equiv 0$. For definiteness, here we consider the case of $\delta > 0$ with the gain (loss) region $x < 0$ ($x > 0$).

In the present study, the simulations are carried out for different values of the perturbation amplitude A and fixed $\beta = 0.5$ and $\delta = 0.1$. The choice of $\beta = 0.5$ makes the hump width comparable to the kink width.

For $\gamma(x) \equiv 0$, we have the integrable SG equation with the following kink solution:

$$\phi_K(x - x_0 - V_kt) = 4\arctan\{\exp[\delta_k(x - x_0 - V_kt)]\}, \tag{4}$$

and the breather solution,

$$\phi_B(x,t) = 4\arctan\frac{\eta\sin\{-\delta_b\omega[t - V_b(x - x_0)]\}}{\omega\cosh[\delta_b\eta(x - x_0 - V_bt)]}, \tag{5}$$

where V_k is the kink velocity, V_b, ω are the breather velocity and frequency, x_0 is the soliton initial position, and

$$\delta_{k,b} = \frac{1}{\sqrt{1 - V_{k,b}^2}}, \quad \eta = \sqrt{1 - \omega^2}. \tag{6}$$

The energy of the kink and the breather are, respectively,

$$E_k = 8\delta_k, \quad E_b = 16\eta\delta_b. \tag{7}$$

Far from the defect, solitons move with constant velocities V_k and V_b feeling no perturbation. In the vicinity of the defect, the soliton parameters change and, as will be shown, it is important from which side the soliton hits the defect.

To study numerically the effect of the perturbation on the dynamics of the SG solitons, we introduce the mesh $x = nh$, where h is the lattice spacing, $n = 0, \pm1, \pm2, \ldots$ and we propose the following discrete version of the model:

$$\begin{aligned}&\frac{d^2\phi_n}{dt^2} - \frac{1}{h^2}(\phi_{n-1} - 2\phi_n + \phi_{n+1}) \\ &\quad + \frac{1}{12h^2}(\phi_{n-2} - 4\phi_{n-1} + 6\phi_n - 4\phi_{n+1} + \phi_{n+2}) \\ &\quad + \sin\phi_n - A\gamma_n\frac{d\phi_n}{dt} = 0,\end{aligned} \tag{8}$$

in which $\phi_n = \phi(nh,t)$ and $\gamma_n = \gamma(nh)$. It can be seen that the term ϕ_{xx} in Eq. (2) is discretized with the accuracy $O(h^4)$, which has already been used by other authors [66,67]. This is done to minimize the effect of discreteness introduced by the mesh. Equations of motion (8) were integrated with respect to the temporal variable using an explicit scheme with the accuracy of $O(\tau^4)$ and the time step τ. The simulations reported below in Sec. IV were conducted for $h = 0.1$ and $\tau = 0.005$.

III. COLLECTIVE VARIABLE METHOD

A collective variable approach has been developed [41] to describe the kink dynamics in the model Eq. (2). The kink is effectively described by the one degree of freedom particle of mass $M = 8$, which is the mass of a standing kink. The kink coordinate $X(t) = x_0 - V_k t$ as a function of time t can be found from the following equation of motion:

$$M\ddot{X} = A\dot{X}f(X), \tag{9}$$

with

$$f(X) = \int_{-\infty}^{\infty}[\phi_K'(x - X)]^2\gamma(x)dx, \tag{10}$$

where the overdot means differentiation with respect to time and the prime denotes differentiation with respect to X. Substituting the kink solution Eq. (4) into Eq. (10), one obtains

$$f(X) = 4\delta_k^2\int_{-\infty}^{\infty}\frac{\gamma(x)dx}{\cosh^2[\delta_k(x - X)]}. \tag{11}$$

The equation of motion (9) was integrated numerically for the initial conditions $X(0) = x_0$, $\dot{X}(0) = V_k$ using the simplest scheme

$$X_{i+1} = \frac{2X_i - (1 + a_i)X_{i-1}}{1 - a_i}, \tag{12}$$

where i denotes the time step number, $a_i = Af_i\tau/(2M)$, $f_i = f(X_i)$, and $\tau = 0.005$ is the time step.

The collective variable equation (9) can also be solved explicitly with its solution given in the form of a quadrature. The first integral reads

$$M\dot{X} = AF(X) + C_1, \tag{13}$$

where

$$F(X) = \int_0^X f(t)dt, \tag{14}$$

and C_1 is the integration constant. The second integration gives

$$\int_0^X \frac{Mdz}{AF(z) + C_1} = t + C_2, \tag{15}$$

with the integration constant C_2. Equation (15) gives the solution to Eq. (9) in an implicit form $t = t(X)$.

A. The kink's phase shift due to interaction with the defect

The kink approaching the defect from the gain (loss) side is first accelerated (decelerated) and then decelerated (accelerated) when it enters the lossy (gain) side. As a result, the kink experiences a phase shift. To calculate the phase shift, we substitute Eq. (11) into Eq. (14):

$$F(X) = \int_0^X ds\int_{-\infty}^{\infty}\frac{\Gamma(x)dx}{\cosh^2[\delta_k(x - s)]}, \tag{16}$$

where $\Gamma(x) = 4\delta_k^2\gamma(x)$. The function

$$f(s) = \int_{-\infty}^{\infty}\frac{\Gamma(x)dx}{\cosh^2[\delta_k(x - s)]} \tag{17}$$

is odd and hence the function $F(X)$ is even. Note that $f(s)$ decays exponentially when $s \to \pm\infty$. From the last statement, we obtain the existence and the equality of the following limits:

$$B = \lim_{s\to+\infty} F(s) = \lim_{s\to-\infty} F(s), \tag{18}$$

where B is the value of the limits.

Coming back to Eq. (15), we note that the integrand can be presented as the sum

$$\frac{M}{AF(z) + C_1} = \frac{M}{AB + C_1} + \frac{MA[B - F(z)]}{[AF(z) + C_1](AB + C_1)}. \tag{19}$$

Substitution of the last equation into Eq. (15) gives

$$\frac{MX(t)}{AB + C_1} + \int_0^X \frac{MA[B - F(z)]}{[AF(z) + C_1](AB + C_1)}dz = t + C_2. \tag{20}$$

The integral in Eq. (20) is bounded uniformly in X since the integrand decays exponentially at infinity. The right-hand side in (20) is a linear function in t. Hence, as $t \to \pm\infty$, each solution to Eq. (9) should behave as

$$X(t) = V_k t + O(1), \tag{21}$$

where $O(1)$ indicates terms bounded as $t \to \pm\infty$, and V_k is in fact the kink velocity given by the formula

$$\frac{1}{V_k} = \frac{M}{AB + C_1}. \tag{22}$$

The last equation expresses the kink velocity in terms of the model parameters. Below we assume that $V_k > 0$, and the case of $V_k < 0$ can be treated in a similar way.

The function $X(t)$ [Eq. (21)] grows at infinity linearly and hence the integral on the left-hand side of (20) tends to a constant as $t \to \pm\infty$. Thus, we can specify behavior of Eq. (21) as follows:

$$X(t) = V_k t + x_\pm + o(1), \quad t \to \pm\infty, \tag{23}$$

where now the symbol $o(1)$ stands for the terms vanishing as $t \to \pm\infty$.

The quantity $\Delta x = x_+ - x_-$ is in fact the kink's phase shift due to the defect, which we now calculate. To do it, we substitute Eq. (23) into Eq. (20), taking into consideration Eq. (22):

$$\frac{x_\pm}{V_k} + o(1) + \frac{1}{V_k}\int_0^{X(t)} \frac{A[B - F(z)]}{AF(z) + C_1} dz = C_2. \tag{24}$$

In the limit $t \to \pm\infty$, for positive V_k one has $X(t) \to \pm\infty$, and Eq. (24) becomes

$$\frac{x_\pm}{V_k} + \frac{1}{V_k}\int_0^{\pm\infty} \frac{A[B - F(z)]}{AF(z) + C_1} dz = C_2. \tag{25}$$

Subtracting one identity from the other one gives

$$\Delta x = x_+ - x_- = -\int_{-\infty}^{+\infty} \frac{A[B - F(z)]}{AF(z) + C_1} dz. \tag{26}$$

The integration constant C_1 can be found from Eq. (22), which allows us to rewrite Eq. (26) as

$$\Delta x = \int_{-\infty}^{+\infty} \frac{A[F(z) - B]}{A[F(z) - B] + MV_k} dz. \tag{27}$$

If $V_k < 0$, the corresponding formula reads

$$\Delta x = -\int_{-\infty}^{+\infty} \frac{A[F(z) - B]}{A[F(z) - B] + MV_k} dz. \tag{28}$$

For the kink solution (4), the function $F(z) - B$ can be cast into the particular form

$$F(z) - B = -\int_z^{+\infty} ds \int_{-\infty}^{+\infty} \frac{\Gamma(x)dx}{\cosh^2[\delta_k(x - s)]}. \tag{29}$$

After changing the order of integration and integrating over s, one obtains

$$F(z) - B = -\delta_k^{-1}\int_{-\infty}^{+\infty} \Gamma(x)\{1 - \tanh[\delta_k(z - x)]\}dx. \tag{30}$$

The kink's phase shift can now be found from Eqs. (27), (28), and (30) by evaluating the integrals numerically.

B. Critical kink velocity

If the kink approaches the defect from the loss side, it must have sufficient momentum not to be trapped. The critical kink initial velocity V_c can be found with the help of the collective variable method. One can present Eq. (9) for $\dot{X}$ in the form

$$M(\dot{X} - \dot{X}_0) = A\int_{-\infty}^{\infty}\int_{X_0}^{X} \frac{\Gamma(x)dx\,dX}{\cosh^2[\delta_k(x - X)]}. \tag{31}$$

A kink having critical velocity must have $\dot{X} = 0$ at $X = 0$, i.e., the kink stops when it reaches the center of the defect.

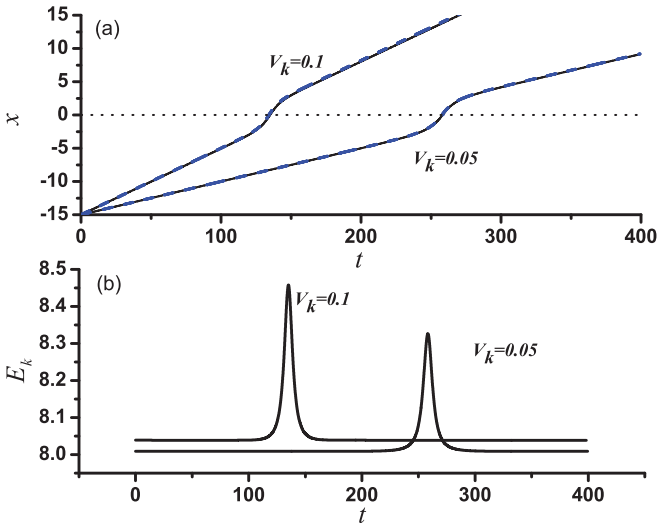

FIG. 1. (Color online) (a) Kink position as a function of time for the two values of kink initial velocity $V_k = 0.05$ and 0.1, for the case in which the kink approaches the defect from the gain side. The defect center is located at $x = 0$. Solid lines show the results of the numerical solution for the continuous system, and dashed lines show the results obtained with the help of the collective variable method. The horizontal dotted line shows the location of the defect center. (b) Time evolution of the kink total energy with the initial velocities $V_k = 0.05$ and 0.1 during the interaction with the defect. The perturbation amplitude is $A = 1.5$ in both cases.

Setting in Eq. (31) $V_c = \dot{X}_0$ and $\dot{X} = 0$ after integrating over the collective variable X, we have

$$V_c = \frac{A}{\delta_k M}\int_{-\infty}^{\infty} \Gamma(x)\{\tanh[\delta_k(x - X_0)] - \tanh[\delta_k(x - X)]\}dx. \tag{32}$$

The value of the integral in Eq. (32) can be found numerically for the initial condition $X_0 = 15$ and recalling that the final stopping point is $X = 0$. For $\beta = 0.5$ and $\delta = 0.1$ used in our study, one finds $V_c = 0.3066(4A/\delta_k M)$. For small kink velocity, $\delta_k = 1$ and $M = 8$ so that

$$V_c = 0.1533A. \tag{33}$$

IV. NUMERICAL RESULTS

A. Kink-defect interaction

First we start with the case of the kink-defect interaction, which is simpler. In Fig. 1, the results for the case when the kink approaches the defect with $A = 1.5$ from the gain side are presented. In Fig. 1(a), the kink position as a function of time is shown by the solid lines for the two values of the initial kink velocity, $V_k = 0.05$ and 0.1, as indicated for each curve. Dashed lines give the results obtained with the help of the theoretical collective variable method, Eq. (12). One can see that the collective variable approach gives a very accurate prediction of the actual kink dynamics. In Fig. 2(b), the time evolution of the kink energy E_k is plotted. From Fig. 1 it is clearly seen that the kink moving toward the defect from the gain side is first accelerated, and after passing the gain side of the defect it is decelerated by the loss side. After the kink passes

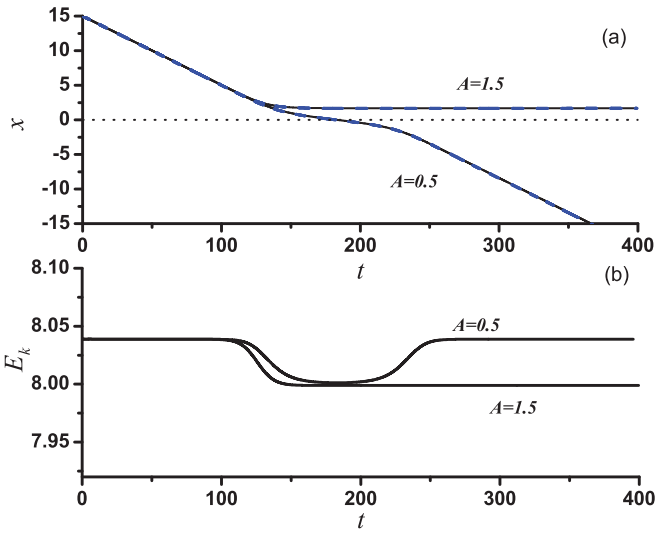

FIG. 2. (Color online) (a) Kink position as a function of time for the case in which the kink approaches the defect from the loss side. The kink velocity is $V_k = -0.1$ and the results are given for $A = 0.5$ and 1.5. The results for the full system described by the partial differential equation (PDE) of Eq. (2) (solid lines) and the ordinary differential equation (ODE) of the collective variable approach (dashed lines) are compared. The dotted line shows the location of the defect center. (b) Time evolution of the kink total energy for the same two cases.

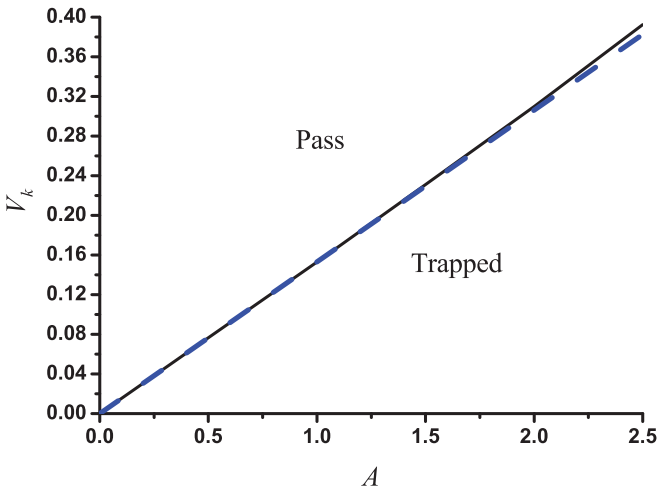

FIG. 3. (Color online) Relation between the critical initial velocity of the kink and the critical defect amplitude. Below the line $V_k = 0.153A$, the kink approaching the defect from the lossy side is always trapped there. Above the line, it passes through the defect and restores its initial velocity. The solid line is for the continuum system, while the dashed line is for the collective variable method.

the defect and moves far from it, it restores its initial velocity and energy. The only effect of the kink-defect interaction in this case is a phase shift. The maximal kink energy increases with an increase in the kink initial velocity V_k for fixed defect amplitude A because of the nature of the defect, whose effect is stronger for larger ϕ_t.

Next, suppose a kink comes from the lossy side. In this case, two different scenarios for the kink interaction with the defect are possible, depending on its initial velocity V_k (or perturbation strength A) as presented in Fig. 2. If V_k is large enough (or A is small enough), the kink passes through the lossy part of the defect with the velocity smaller than V_k, and it enters the gain part where it is accelerated up to the initial velocity and then goes on to infinity. In the opposite case (where V_k is not large enough or A is not small enough), the kink does not possess sufficient momentum to pass through the lossy part of the defect, and it is trapped there. In Fig. 2(a), the kink position as a function of time is shown for $A = 0.5$ and 1.5 with $V_k = -0.1$ in both cases. Figure 2(b) shows the kink total energy as a function of time for these two cases. As one can see, for the case of $A = 0.5$ the kink passes through the defect and restores its initial velocity, while for $A = 1.5$ the kink is trapped by the lossy side of the defect.

We now further expand on our comparison of the kink dynamics observed in the continuous PDE system of Eq. (2) with that in the single degree of freedom ODE model of Eq. (9). In Fig. 3, the plane of the parameters A and V_k is shown with the line that separates the two possible scenarios of the kink-defect interaction when the kink approaches the defect from the lossy side. Above the line the kink has sufficient initial momentum to pass through the defect and to restore its initial velocity. Contrary to this, below the line the kink is always trapped in the lossy region of the defect and eventually stops. The collective variable result Eq. (33) is shown by the dashed line. The result obtained for the continuum system (shown by the solid line) is in perfect agreement with the collective variable method for small kink velocity, and the deviation increases for larger kink velocities. This is natural to expect as the collective coordinate derivation of [41] was obtained away from the relativistic regime of large speeds V_k. Nevertheless, we observe that for speeds even nearly half the maximal speed of propagation in the medium, the relevant collective coordinate prediction remains very accurate.

In Fig. 4, the kink's phase shift due to interaction with the $\mathcal{PT}$-symmetric defect is presented as a function of its initial velocity. Solid lines show the results of the numerical solution for the continuous system, and dashed lines show the results obtained with the help of the collective variable method of Eqs. (27), (28), and (30). In Fig. 4(a), the kink moves toward the defect with strength $A = 0.5$ from the gain side. In Fig. 4(b), the kink moves from the opposite side and $A = 0.1$. The vertical dotted line shows the critical value of the initial kink velocity for this case. It can be seen that the accuracy of the collective variable method is very high, especially for small V_k. The plots show a smaller phase shift for higher kink initial velocity. This comes from the fact that a higher velocity kink is more accelerated by the perturbation considered here.

B. Kink-kink-defect interaction

Here we demonstrate that the kink K_1 trapped at the lossy side of the defect can be pushed through the defect by the second kink K_2 even if the second kink has velocity smaller than the threshold value. To do so, we consider two well-separated kinks moving with the same velocity below the threshold value toward the lossy side of the defect. The first kink is trapped and the second one pushes it, through their well-known mutual repulsion [67], through the defect being

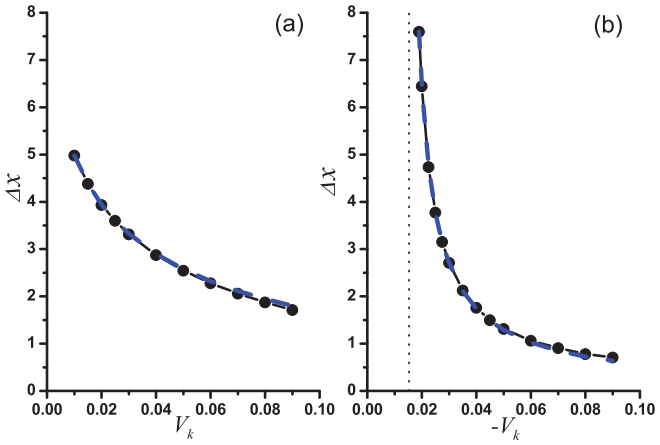

FIG. 4. (Color online) Kink's phase shift due to the interaction with a $\mathcal{PT}$-symmetric defect as a function of its initial velocity for the kink moving (a) toward the gain side of the defect with strength $A = 0.5$ and (b) toward the lossy side of the defect with strength $A = 0.1$. Solid lines show the results of numerical solution for the continuous PDE system, and dashed lines show the results obtained with the help of the collective variable ODE method, Eqs. (27), (28), and (30). The vertical dotted line in (b) shows the threshold kink velocity $V_c = -0.0153$.

either reflected back [see Fig. 5(a) for the case of $V_k = -0.06$] or trapped itself [as in Fig. 5(b) for the case of $V_k = -0.07$]. Note that the threshold kink velocity is $V_c = -0.0765$ for $A = 0.5$, used for this simulation.

C. Breather-defect interaction

It was found that the result of the breather-defect interaction depends on the initial breather position x_0, because this

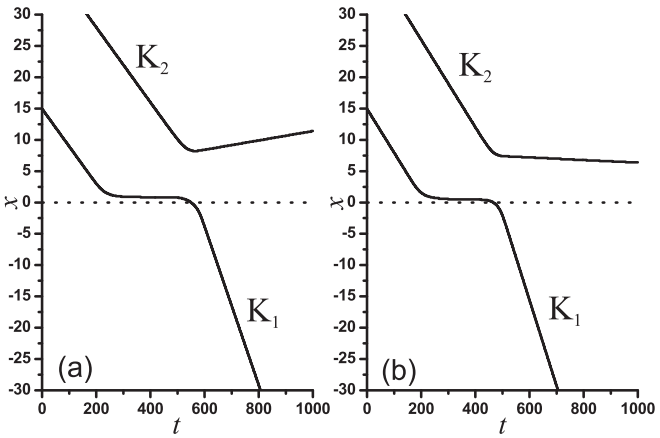

FIG. 5. Dynamics of the two well-separated kinks moving toward the defect from the lossy side with a velocity smaller than the threshold value. K_1 is trapped by the defect and then it is pushed through the defect by K_2, through their mutual repulsion. In (a), K_2 is reflected, while in (b) it is trapped by the lossy region of the defect. Horizontal dashed lines show the location of the center of the defect. Here (a) $V_k = -0.06$, (b) $V_k = -0.07$, and $A = 0.5$ in both cases. The threshold kink velocity is $V_c = -0.0765$. The kink initial positions are $x_0 = 15$ for K_1 and $x_0 = 40$ for K_2.

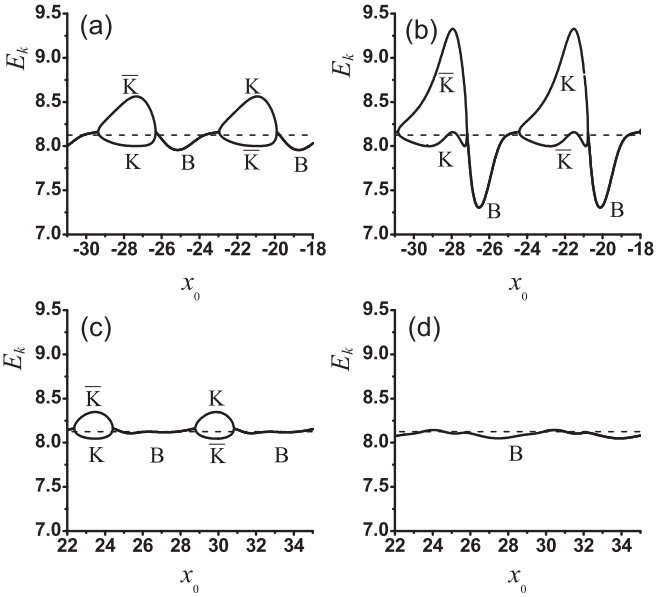

FIG. 6. Numerical results for the breather interaction with the $\mathcal{PT}$-symmetric defect in the perturbed SGE model Eq. (2) for the breather approaching (a) and (b) from the gain side of the defect and (c) and (d) from the lossy side of the defect. Shown are the total energies of the subkinks constituting the breather under the assumption that they share the breather energy equally. When the breather splits into a kink-antikink pair, the subkinks have different energies and the lines split into two. The defect amplitude is $A = 0.1$ in (a) and (c) and $A = 0.4$ in (b) and (d). The breather has initial velocity $V_b = \pm 0.2$ and frequency $\omega = 0.1$.

parameter controls the breather oscillation phase at which it hits the defect. A moving breather in one oscillation travels the distance $\lambda = 2\pi\delta_b|V_b|/\omega$. This means that it is sufficient to consider the range of the initial breather positions from x_0 to $x_0 + \lambda$. In some cases, the breather can split into a kink and an antikink after passing the defect. In this situation, it is convenient to present the result of the breather-defect interaction by the total energies of the subkinks constituting the breather under the assumption that the subkinks, when merged into a resulting breather after the interaction, share the breather energy equally. In the cases in which the breather splits into a kink-antikink pair, the energies of the subkinks are different and they are calculated after they become well-separated.

In Fig. 6, we plot the total energy of the subkinks after the breather collides with the defect as a function of its initial position x_0. Horizontal dashed lines show the initial energy of the subkinks. In Figs. 6(a) and 6(b), we show the case in which the breather approaches the defect from the gain side, and in Figs. 6(c) and 6(d) it moves toward the defect from the opposite direction. In Figs. 6(a) and 6(c), the defect amplitude is $A = 0.1$, while in Figs. 6(b) and 6(d), $A = 0.4$. The breather has frequency $\omega = 0.1$ and the initial velocity of $V_b = \pm 0.2$, so that in all cases $\lambda = 12.83$. The plots include the whole period of the breather initial position. One can see that in Figs. 6(a)–6(c) there exist the domains of x_0 where the breather (B) splits into a kink-antikink (K-$\overline{K}$) pair. In (d) the breather does not gain enough energy from the defect to split. It can be concluded that the breather can split regardless

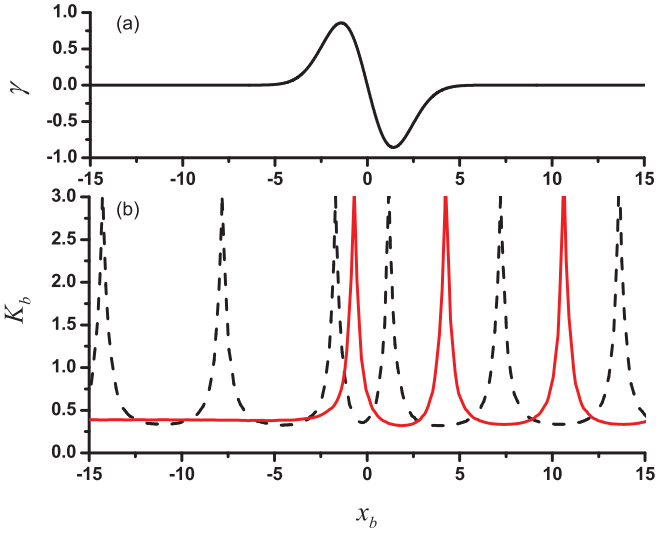

FIG. 7. (Color online) (a) γ as the function of x. (b) The kinetic energy of the breather as a function of its position. The breather comes from the lossy (positive x_b, i.e., right end) side of the defect toward the gain (negative x_b, i.e., left end) side with initial positions $x_0 = 23.5$ (solid line) and $x_0 = 26.5$ (dashed line) [see Fig. 6(c)]. In both cases, $V_b = -0.2$, $\omega = 0.1$, and $A = 0.1$.

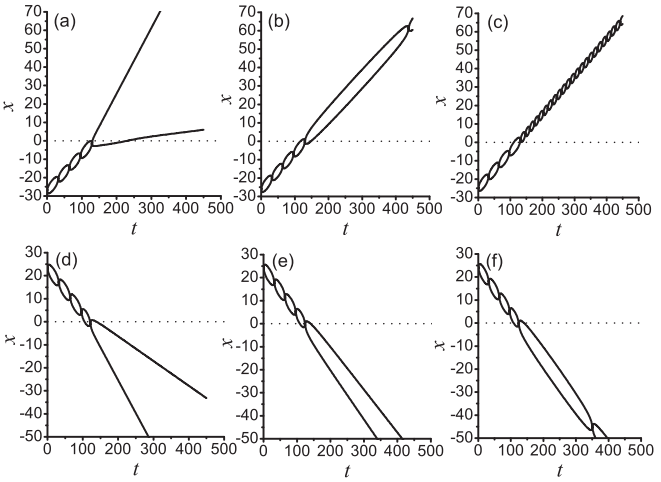

FIG. 8. Examples of breather dynamics during the interaction with the defect of strength $A = 0.1$. In (a)–(c) the breather moves toward the defect from the gain side, and in (d)–(f) from the loss side. Initial breather parameters are $\omega = 0.1$, $V_b = \pm 0.2$, and initial positions are (a) $x_0 = -27.34$, (b) $x_0 = -26.32$, (c) $x_0 = -25.16$, (d) $x_0 = 23.48$, (e) $x_0 = 24.40$, and (f) $x_0 = 24.42$. Horizontal dashed lines show the position of the defect center, and wavy lines represent the breather's two subkinks.

of the direction in which it approached the defect. However, the maximal energy gain is larger when the breather moves toward the gain side of the defect. It is also interesting that, although there are (naturally expected) cases in which the splinters bear a lower energy sum than that of the original breather, there are also cases in which their sum exceeds the energy of the original breather. Again, this can happen on either side of the approach, although it is again more pronounced when approaching the defect from the gain side.

To explain the dependence of the breather-defect interaction on the breather phase, we note that the kinetic energy of the moving breather is a periodic function of time and space with the sharp maxima at the points where the subkinks collide. The perturbation term in Eq. (2), as was already mentioned, acts more prominently for large ϕ_t. Thus, the location of the subkink collision points with respect to the maximum and minimum of $\gamma(x)$ is very important. In Fig. 7(a), the function $\gamma(x)$ is shown. In Fig. 7(b), the breather kinetic energy K_b as a function of its spatial coordinate x_b is given for the two cases, $x_0 = 23.5$ (solid line) and $x_0 = 26.5$ (dash line), for $V_b = -0.2$ and $\omega = 0.1$, which corresponds to Fig. 6(c). The perturbation strength is $A = 0.1$. In both cases, the breather moves from the right to the left and approaches the defect from the loss side. The solid line shows the case when the maxima of the kinetic energy almost do not catch the lossy region of the defect, but one of the maxima takes place near the maximum of the gain region. As a result, the breather gains more energy than it loses and it splits into a kink-antikink pair, so that the kinetic energy does not oscillate after the breather passes the defect. The dashed line shows the case in which one maximum of the breather's kinetic energy nearly fits to the maximal loss and the next maximum nearly fits to the maximal gain. In this case, the breather passes through the defect almost unchanged. Hence, clearly the interplay of the kinetic energy oscillation with the spatial distribution of the gain-loss profile is critical in determining the observed breather-defect interaction phenomenology.

For large perturbations (i.e., stronger defects), the maxima of the kinetic energy always catch the lossy region of the defect. Consequently, the breather does not gain more energy than it loses and it never splits into a kink-antikink pair for any initial position of the breather [see Fig. 6(d)].

Examples of the breather interaction with the defect are presented in Fig. 8 for different initial breather positions. In Figs. 8(a)–8(c), the breather approached the defect from the gain side, and in Figs. 8(d)–8(f) from the loss side. The breather parameters are $V_b = \pm 0.2$ and $\omega = 0.1$ and the perturbation amplitude is $A = 0.1$ in all cases. In Figs. 8(a), 8(d), and 8(e), the breather breaks up into subkinks. The breaking up takes place only for breathers with sufficiently small frequencies. In Figs. 8(b) and 8(f) after the interaction of the defect, the breather frequency decreases, which means that the breather total energy increases. In Fig. 8(c), the breather frequency increases (total energy decreases). This again corroborates the fact that the breather may either lose or gain energy upon its interaction with the defect (contrary to what we saw, e.g., in the case of the kink).

D. Kink-antikink-defect interaction

In Fig. 9, we present the results obtained for the case when a well-separated antikink and kink move toward the defect with the velocity V_k from the lossy side. The defect strength is $A = 0.5$, and thus the kink critical velocity is $V_c = -0.0765$. We take (a) $V_k = -0.06$, (b) $V_k = -0.075$, (c) $V_k = -0.068$, and (d) $V_k = -0.088$, so that in the first three cases $V_k < V_c$ and the antikink is trapped at the lossy region. Then the kink approaches the antikink and they create

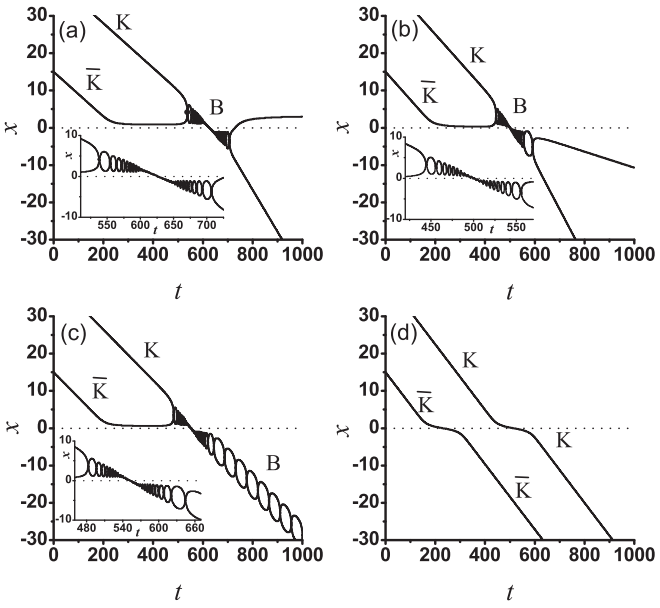

FIG. 9. Examples of the interaction of a kink-antikink pair with a defect of strength $A = 0.5$. In all cases, the kink and antikink move toward the defect from the loss side with equal velocity. Horizontal dashed lines show the location of the center of the defect. In (a)–(c) the velocity of the kinks is smaller than the threshold value $V_c = -0.0765$: (a) $V_k = -0.06$, (b) $V_k = -0.075$, (c) $V_k = -0.068$, while in (d) $V_k = -0.088$, i.e., both have velocities above the threshold value and overcome the defect, effectively without interacting. The kink initial positions are $x_0 = 15$ for $\overline{K}$ and $x_0 = 40$ for K. The insets show the details of the dynamics close to the defect center.

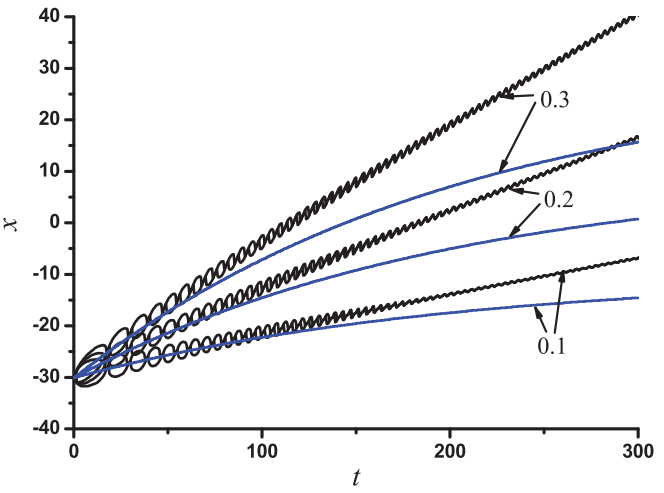

FIG. 10. (Color online) Dynamics of breathers and kinks with initial velocities equal to 0.1, 0.2, and 0.3 in the case of homogeneous loss $\gamma(x) \equiv 1$ and $A = -0.005$. The breather initial frequency is $\omega = 0.1$. The kink trajectories (smooth lines) show that kink propagation velocity gradually decreases, while breather trajectories (wavy lines) demonstrate almost constant propagation velocities, i.e., minimal impact in the breather translation by the presence of the dissipative perturbation.

a breather. Interestingly, the breather easily enters the gain side of the defect and it is amplified. In Fig. 9(a), the breather splits into a kink-antikink pair with one subkink trapped by the loss region and another one passing through the defect. In Fig. 9(b), both subkinks pass through the defect. In Fig. 9(c), the breather does not split and it moves away from the defect as a single entity (i.e., the antikink and kink remain bound). In Fig. 9(d), $V_k > V_c$ and the antikink is not trapped by the defect, and both subkinks pass through the defect effectively without interacting with each other.

Note that in Fig. 9(b) both the kink and antikink have $V_k < V_c$, nevertheless they *both* pass through the defect. Two reasons can be given to explain this effect, and they both are related to the fact that the kink and antikink form a breather to pass through the defect. In Sec. IV C, it was shown that the breather can gain energy from the $\mathcal{PT}$-symmetric defect, depending on the phase, and this is the first reason. The second reason is that the breather translational degree of freedom is only weakly affected by the perturbation considered in this study. This is demonstrated in Fig. 10, where we contrast the dynamics of breathers and kinks with initial velocities equal to 0.1, 0.2, and 0.3 in the case of homogeneous loss $\gamma(x) \equiv 1$ and $A = -0.005$. The breather initial frequency is $\omega = 0.1$. It can be seen that the kink trajectories (smooth lines) show that kink propagation velocity gradually decreases, while breather trajectories (wavy lines) demonstrate almost constant propagation velocities. Hence, this suggests that while kinks are topologically robust, breathers are more efficient in weathering lossy media and in overcoming barriers imposed by dissipative perturbations. This is a feature that is especially useful in the realm of $\mathcal{PT}$-symmetric perturbations/defects.

V. CONCLUSIONS

Interaction of SG kinks (and multikinks) as well as breathers with a $\mathcal{PT}$-symmetric defect bearing balanced regions of positive and negative dissipation of energy was investigated analytically (wherever possible) and numerically in the present work.

It was demonstrated that a kink coming from the gain side always passes through the defect and restores its initial velocity (see Fig. 1). The only effect of the interaction with the defect is a phase shift associated with the kink position. However, for the kink approaching the defect from the opposite side, there exist two different scenarios, depending on the kink initial velocity V_k. For $V_k < V_c$, where V_c is a threshold value of the velocity, the kink does not have enough energy to pass through the defect, and it is trapped by the lossy side of the defect (see Fig. 2), while for $V_k > V_c$ it is able to overcome the relevant barrier.

If two well-separated kinks approach the defect from the lossy side with the velocities less than V_c, then one of them can pass through the defect while another one will be either trapped by the lossy region or reflected back (see Fig. 5), i.e., their pairwise repulsion may modify the collisional outcome with the defect.

The breather-defect interaction is more interesting since the breather can split into subkinks depending on its parameters and also on the amplitude of the defect. Depending on the breather initial phase, its total energy can be increased or decreased after the interaction with the defect (see Figs. 6 and 8). This can be explained by the fact that the kinetic energy

of the moving breather is a periodic function of time and space with sharp maxima at the points where the subkinks collide. The type of perturbation considered in the present work is more prominent for large ϕ_t. Change in the breather phase changes the location of the subkink collision points with respect to the maxima of the gain and loss regions, thus affecting the overall result of the interaction between the breather and the defect (see Fig. 7).

A well-separated kink and antikink pair moving toward the lossy side of the defect with $V_k < V_c$, may enable *both* coherent structures to potentially pass through the defect [see Fig. 9(b)]. This happens because the kink and antikink form a breather that can gain energy from the defect and whose propagation velocity is less affected by the dissipative term than the propagation velocity of the constituent kink or antikink (see Fig. 10).

We conclude that the $\mathcal{PT}$-symmetric defects give new opportunities in the manipulation with the soliton dynamics in the sine-Gordon equation and related field theories. Numerous future directions open up as a result of the present considerations. One such direction is to consider other Klein-Gordon field theories in the presence of $\mathcal{PT}$-symmetric defects, such as, e.g., the ϕ^4 model. The latter is especially interesting due to the presence of internal modes in the kink dynamics, which may have a nontrivial impact on the observed phenomenology. Another relevant consideration is that of higher dimensionality. Examining radial kinks as well as breathers in the higher-dimensional versions of the sine-Gordon model is a theme that has attracted recent interest [68], including the formation of breathers as a result of the interaction of the kinks with a radial domain boundary. Developing $\mathcal{PT}$-symmetric variants of the two-dimensional sine-Gordon model and examining the corresponding dynamics is still an open problem. It is also relevant to analyze $\mathcal{PT}$-symmetric defects with different profiles. Of particular interest is a $\gamma(x)$ with a compact support, being nonzero in $-\alpha < x < \alpha$ and $\gamma(x) = 0$ if $|x| \geqslant \alpha$, as well as a $\gamma(x)$ bearing a (truncated) periodic structure. In the compactly supported case, one may envision different regimes of solitary-wave–defect interaction, possibly including a reflection one. Finally, comparison of the present features with corresponding bright and dark soliton interactions with $\mathcal{PT}$-symmetric defects within the realm of the focusing and defocusing $\mathcal{PT}$-symmetric nonlinear Schrödinger equation, respectively, would also be a theme of relevance to future studies, especially since the latter is the principal field of optical applications of $\mathcal{PT}$-symmetric models. Such studies are presently under consideration and will be reported in future publications.

ACKNOWLEDGMENTS

D.S. gratefully acknowledges the hospitality of the Bashkir State Pedagogical University and the Institute for Metals Superplasticity Problems, Ufa, Russia. S.V.D. gratefully acknowledges financial support provided by the Government Program 5-100-2020. D.I.B. was partially supported by a grant from the Russian Foundation for Basic Research, the grant of the President of Russian Federation for young scientists-doctors of science (project no. MD-183.2014.1), and by the fellowship of Dynasty Foundation for young Russian mathematicians. P.G.K. acknowledges support from the U.S. National Science Foundation under Grants No. CMMI-1000337 and No. DMS-1312856, from the ERC and FP7-People under Grant No. IRSES-606096 from the Binational (U.S.-Israel) Science Foundation through Grant No. 2010239, and from the U.S.-AFOSR under Grant No. FA9550-12-10332.

[1] C. M. Bender and S. Boettcher, Phys. Rev. Lett. **80**, 5243 (1998).
[2] C. M. Bender, D. C. Brody, and H. F. Jones, Phys. Rev. Lett. **89**, 270401 (2002).
[3] Y. C. Lee, M. H. Hsieh, S. T. Flammia, and R. K. Lee, Phys. Rev. Lett. **112**, 130404 (2014).
[4] C. E. Ruter, K. G. Markris, R. El-Ganainy, D. N. Cristodoulides, M. Segev, and D. Kip, Nat. Phys. **6**, 192 (2010).
[5] A. Guo, G. J. Salamo, D. Duchesne, R. Morandotti, M. Volatier-Ravat, V. Aimez, G. A. Siviloglou, and D. N. Christodoulides, Phys. Rev. Lett. **103**, 093902 (2009).
[6] A. Regensburger, C. Bersch, M. A. Miri, G. Onishchukov, D. N. Christodoulides, and U. Peschel, Nature (London) **488**, 167 (2012).
[7] A. Regensburger, M. A. Miri, C. Bersch, J. Nager, G. Onishchukov, D. N. Christodoulides, and U. Peschel, Phys. Rev. Lett. **110**, 223902 (2013).
[8] B. Peng, S. K. Ozdemir, F. Lei, F. Monifi, M. Gianfreda, G. L. Long, S. Fan, F. Nori, C. M. Bender, and L. Yang, Nat. Phys. **10**, 394 (2014).
[9] J. Schindler, A. Li, M. C. Zheng, F. M. Ellis, and T. Kottos, Phys. Rev. A **84**, 040101 (2011).
[10] J. Schindler, Z. Lin, J. M. Lee, H. Ramezani, F. M. Ellis, and T. Kottos, J. Phys. A **45**, 444029 (2012).
[11] N. Bender, S. Factor, J. D. Bodyfelt, H. Ramezani, D. N. Christodoulides, F. M. Ellis, and T. Kottos, Phys. Rev. Lett. **110**, 234101 (2013).
[12] C. M. Bender, B. Berntson, D. Parker, and E. Samuel, Am. J. Phys. **81**, 173 (2013).
[13] M. C. Zheng, D. N. Christodoulides, R. Fleischmann, and T. Kottos, Phys. Rev. A **82**, 010103 (2010).
[14] S. Longhi, Phys. Rev. A **81**, 022102 (2010).
[15] H. Cartarius and G. Wunner, Phys. Rev. A **86**, 013612 (2012); J. Phys. A **45**, 444008 (2012).
[16] E.-M. Graefe, J. Phys. A **45**, 444015 (2012).
[17] A. S. Rodrigues, K. Li, V. Achilleos, P. G. Kevrekidis, D. J. Frantzeskakis, and C. M. Bender, Rom. Rep. Phys. **65**, 5 (2013).
[18] V. Achilleos, P. G. Kevrekidis, D. J. Frantzeskakis, and R. Carretero-González, Phys. Rev. A **86**, 013808 (2012).
[19] H. Ramezani, T. Kottos, V. Kovanis, and D. N. Christodoulides, Phys. Rev. A **85**, 013818 (2012).
[20] A. E. Miroshnichenko, B. A. Malomed, and Yu. S. Kivshar, Phys. Rev. A **84**, 012123 (2011).
[21] C. T. West, T. Kottos, and T. Prosen, Phys. Rev. Lett. **104**, 054102 (2010).
[22] A. A. Sukhorukov, S. V. Dmitriev, S. V. Suchkov, and Yu. S. Kivshar, Opt. Lett. **37**, 2148 (2012).

[23] F. Nazari, M. Nazari, and M. K. Moravvej-Farshi, Opt. Lett. **36**, 4368 (2011).
[24] J. D'Ambroise, P. G. Kevrekidis, and S. Lepri, J. Phys. A **45**, 444012 (2012).
[25] J. D'Ambroise, S. Lepri, B. A. Malomed, and P. G. Kevrekidis Phys. Lett. A **378**, 2824 (2014).
[26] I. V. Barashenkov, S. V. Suchkov, A. A. Sukhorukov, S. V. Dmitriev, and Yu. S. Kivshar, Phys. Rev. A **86**, 053809 (2012).
[27] S. V. Suchkov, S. V. Dmitriev, A. A. Sukhorukov, I. V. Barashenkov, E. R. Andriyanova, K. M. Badgetdinova, and Yu. S. Kivshar, Appl. Phys. A **115**, 443 (2014).
[28] L. Kh. Rysaeva, S. V. Suchkov, and S. V. Dmitriev, JETP Lett. **99**, 577 (2014).
[29] S. V. Dmitriev, S. V. Suchkov, A. A. Sukhorukov, and Yu. S. Kivshar, Phys. Rev. A **84**, 013833 (2011).
[30] S. V. Suchkov, S. V. Dmitriev, B. A. Malomed, and Yu. S. Kivshar, Phys. Rev. A **85**, 033825 (2012).
[31] S. V. Suchkov, A. A. Sukhorukov, S. V. Dmitriev, and Yu. S. Kivshar, Europhys. Lett. **100**, 54003 (2012).
[32] K. Li and P. G. Kevrekidis, Phys. Rev. E **83**, 066608 (2011).
[33] I. V. Barashenkov, G. S. Jackson, and S. Flach, Phys. Rev. A **88**, 053817 (2013).
[34] J. Pickton and H. Susanto, Phys. Rev. A **88**, 063840 (2013).
[35] P. G. Kevrekidis, D. E. Pelinovsky, and D. Y. Tyugin, SIAM J. Appl. Dyn. Sys. **12**, 1210 (2013).
[36] P. G. Kevrekidis, D. E. Pelinovsky, and D. Y. Tyugin, J. Phys. A **46**, 365201 (2013).
[37] D. E. Pelinovsky, D. A. Zezyulin, and V. V. Konotop, J. Phys. A **47**, 085204 (2014).
[38] K. Li, P. G. Kevrekidis, B. A. Malomed, and U. Günther, J. Phys. A **45**, 444021 (2012).
[39] N. V. Alexeeva, I. V. Barashenkov, K. Rayanov, and S. Flach, Phys. Rev. A **89**, 013848 (2014).
[40] H. Xu, P. G. Kevrekidis, and A. Saxena, arXiv:1404.4382.
[41] P. G. Kevrekidis, Phys. Rev. A **89**, 010102 (2014).
[42] J. Cuevas, L. Q. English, P. G. Kevrekidis, and M. Anderson, Phys. Rev. Lett. **102**, 224101 (2009).
[43] A. Demirkaya, D. J. Frantzeskakis, P. G. Kevrekidis, A. Saxena, and A. Stefanov, Phys. Rev. E **88**, 023203 (2013).
[44] A. Demirkaya, T. Kapitula, P. G. Kevrekidis, M. Stanislavova, and A. Stefanov, Stud. Appl. Math. **133**, 298 (2014).
[45] N. Lu, P. G. Kevrekidis, and J. Cuevas-Maraver, J. Phys. A: Math. Theor. **47**, 455101 (2014).
[46] S. V. Dmitriev and P. G. Kevrekidis, *Soliton Collisions, in The Sine-Gordon Model and Its Applications*, edited by J. Cuevas-Maraver, P. G. Kevrekidis, and F. Williams (Springer, Cham, 2014), pp. 59–95.
[47] S. V. Dmitriev, Yu. S. Kivshar, and T. Shigenari, Phys. Rev. E **64**, 056613 (2001).
[48] S. V. Dmitriev, P. G. Kevrekidis, and Yu. S. Kivshar, Phys. Rev. E **78**, 046604 (2008).
[49] Yu. S. Kivshar and B. A. Malomed, Phys. Lett. A **129**, 443 (1988).
[50] Yu. S. Kivshar, B. A. Malomed, and A. A. Nepomnyashchy, Zh. Eksp. Teor. Fiz. Sov. Phys. JETP **94**, 356 (1988).
[51] Z. Fei, Yu. S. Kivshar, and L. Vázquez, Phys. Rev. A **45**, 6019 (1992).
[52] Z. Fei, Yu. S. Kivshar, and L. Vázquez, Phys. Rev. A **46**, 5214 (1992).
[53] B. Piette and W. J. Zakrzewski, Phys. Rev. E. **79**, 046603 (2009).
[54] Yu. S. Kivshar, D. E. Pelinovsky, T. Cretegny, and M. Peyrard, Phys. Rev. Lett. **80**, 5032 (1998).
[55] N. R. Quintero and P. G. Kevrekidis, Phys. D **170**, 31 (2002).
[56] Yu. S. Kivshar, Z. Fei, and L. Vázquez, Phys. Rev. Lett. **67**, 1177 (1991).
[57] B. A. Malomed, Phys. D **15**, 385 (1985).
[58] D. K. Campbell, M. Peyrard, and P. Sodano, Phys. D **19**, 165 (1986).
[59] R. H. Goodman and R. Haberman, Phys. Rev. Lett. **98**, 104103 (2007).
[60] D. K. Campbell, J. S. Schonfeld, and C. A. Wingate, Phys. D **9**, 1 (1983).
[61] D. K. Campbell and M. Peyrard, Phys. D **18**, 47 (1986).
[62] R. Scharf, Yu. S. Kivshar, A. Sanchez, and A. R. Bishop, Phys. Rev. A **45**, R5369 (1992).
[63] P. S. Lomdahl, O. H. Olsen, and M. R. Samuelsen, Phys. Rev. A **29**, 350 (1984).
[64] M. Inoue and S. G. Chung, J. Phys. Soc. Jpn. **46**, 1594 (1979).
[65] C. S. Carvalho and L. Perivolaropoulos, Phys. Rev. D **79**, 065032 (2009).
[66] O. M. Braun and Yu. S. Kivshar, *The Frenkel-Kontorova Model: Concepts, Methods, and Applications* (Springer, Berlin, 2004).
[67] Yu. S. Kivshar and B. A. Malomed, Rev. Mod. Phys. **61**, 763 (1989).
[68] J. G. Caputo and M. P. Soerensen, Phys. Rev. E **88**, 022915 (2013).